

Article http://pubs.acs.org/iournal/aesccg

# Probing the Fate of Different Structures of Beta-Lactam Antibiotics: Hydrolysis, Mineral Capture, and Influence of Organic Matter

Annaleise R. Klein, Eirini Sarri, Sabrina E. Kelch, Jade J. Basinski, Shreya Vaidya, and Ludmilla Aristilde\*



Cite This: ACS Earth Space Chem. 2021, 5, 1511-1524



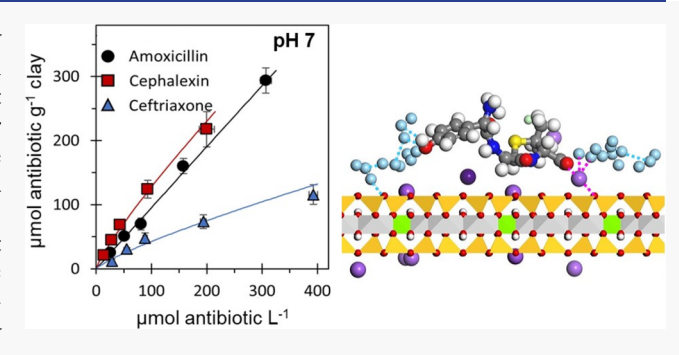
**ACCESS** 

III Metrics & More

Article Recommendations

s Supporting Information

ABSTRACT: Beta-lactam antibiotics, which are used extensively in human and veterinary applications, are commonly detected in surface waters. To examine how the distinct structures of different generations of beta-lactam antibiotics can influence their persistence or degradation in environmental aqueous media, we examined the fate of two penams (amoxicillin and cloxacillin) and two cephems (cephalexin and ceftriaxone) at pH 5.0 and pH 7.0. By contrast to the lack of hydrolysis of the penam antibiotics at both pHs, we observed hydrolysis of cephalexin at pH 7.0 ( $t_{1/2}$  = 12 d) and ceftriaxone at pH 5.0 ( $t_{1/2}$  = 2.8 d). Using highperformance liquid chromatography coupled with a diode array detector or a high-resolution mass spectrometer, we were able to



confirm thiotriazinone and 3-desacetyl cefotaxime as major hydrolysis products of ceftriaxone, and propose the hydrolytic cleavage of the benzene and cephem moieties from cephalexin. In addition, we studied the effects of smectite clay particles suspended in solutions without or with dissolved organic matter. The adsorption capacity of the clay was 4- to 9-fold higher at pH 7.0 than at pH 5.0. Subsequent X-ray diffraction analysis revealed that the antibiotic adsorption was not within the clay interlayer nanopores but occurred primarily on the external clay surfaces. The addition of dissolved organic matter interfered with the adsorption of a cephem antibiotic (ceftriaxone) on the clay, but the adsorption of a penam antibiotic (amoxicillin) remained unaffected. We employed molecular modeling simulations to probe the mechanisms of adsorption on the mineral surface. Our findings offer new insights on how the compound structures can dictate different fates of the beta-lactam class of antibiotics in environmental media.

KEYWORDS: Hydrolysis, clay, organic matter, molecular simulations, montmorillonite, thiotriazinone

## 1. INTRODUCTION

For over 70 years, the beta-lactam ( $\beta$ -lactam) class of antibiotics has been significant in preventative and postinfection treatment applications in human medicine and veterinary practices. <sup>1,2</sup> With over 30 kilotons of  $\beta$ -lactam antibiotics sold globally per year,<sup>3</sup> they are subsequently released into various environmental matrices due to both improper disposal and incomplete metabolism after ingestion.<sup>2,4-7</sup> For instance, it was calculated that up to 74% of penicillin and 79% of cephalosporin administered in hospitals and medical practices were emitted into sewage. Various  $\beta$ lactam antibiotics including cloxacillin, amoxicillin, mezlocillin, flucloxacillin, piperacillin, ampicillin, and oxacillin were detected, from less than 10 ng L<sup>-1</sup> to up to 50 ng L<sup>-1</sup>, in surface water samples collected in Europe and in the United States.<sup>5,6</sup> Due to the broad-spectrum antibacterial activity afforded by their structural diversity,  $\beta$ -lactam antibiotics have become the most used class of antibiotics worldwide. 1,3,9,10 Therefore, there is rising interest in understanding the environmental fate of different antibiotics in the  $\beta$ -lactam

class, especially due to their different chemical structures, acidbase chemistry, and functional groups.

In addition to the prototypical  $\beta$ -lactam ring (a four-member cyclic amide), other structural characteristics have led to the four major categories of  $\beta$ -lactam antibiotics: penams, cephems, carbapenems, and monobactams. 10 The penam antibiotics, to which penicillin, amoxicillin, and cloxacillin belong, represent the oldest and largest category of  $\beta$ -lactam antibiotics. These penam antibiotics are characterized by a  $\beta$ lactam ring fused with a thiazolidine ring and the presence of a side chain at the C6 position (Figure 1A,B). The increased resistance of pathogenic bacteria including Staphylococcus species to penam antibiotics led to the synthesis of alternative  $\beta$ -lactam antibiotics. <sup>10-12</sup> The cephems, which include

Received: March 10, 2021 Revised: April 28, 2021 Accepted: May 12, 2021 Published: June 1, 2021





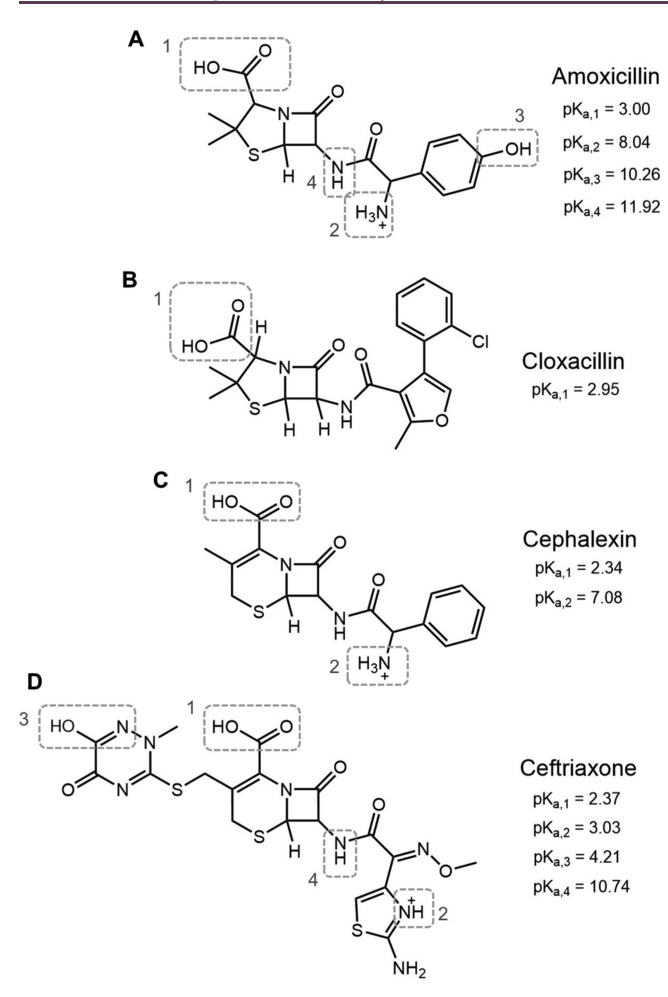


**Figure 1.** Chemical structures of the four β-lactam antibiotics investigated in this study. Penams: (A) amoxicillin and (B) cloxacillin. Cephems: (C) cephalexin and (D) ceftriaxone. The dashed boxes on each compound indicate the ionizable functional groups.

cephalexin and ceftriaxone, differ from the penams by both the replacement of the thiazolidine ring with a dihydrothiazine ring and the placement of the side chains at the C3 and C7 positions (Figure 1C,D). 5,13 The evolution of different generations of cephem antibiotics provided enhanced effectiveness against Gram-negative bacteria. 12 The antibiotics in the carbapenem category, which increase the spectrum of antibacterial action, possess a five-membered ring in addition to the common  $\beta$ -lactam ring. The monobactam antibiotics, which contain only the monocyclic  $\beta$ -lactam ring structure that defines  $\beta$ -lactam antibiotics, represent an alternative for patients allergic to the other  $\beta$ -lactam antibiotics. <sup>10–12,14</sup> Here, to explore the effects of the structural diversity of  $\beta$ -lactam antibiotics on their environmental fate in aqueous media, we investigated hydrolysis, adsorption to mineral particles, and organic matter binding of two penam (amoxicillin and cloxacillin) and two cephem (ceftriaxone and cephalexin)  $\beta$ -lactam antibiotics.

The  $\beta$ -lactam antibiotics are considered to be poorly stable due to the susceptibility of the  $\beta$ -lactam ring to chemical or enzymatic hydrolysis. However, the degradation kinetics of these antibiotics are found to be highly dependent on environmental conditions and the antibiotic structure. A previous study on two different monobactams, whose structures differ by the presence or absence of a (*tert*-

butyldimethylsilanyloxy)ethyl group, reported vastly different degradation kinetics as a function of solution pH.4 The compound without the alkyl-silicon group was degraded most efficiently under alkaline pH, with a half-life  $(t_{1/2})$  of nearly 1 day at pH 9, compared to 9 days at pH 7 and nearly 50 days at pH 3.4 By comparison, the compound with the alkyl-silicon group was degraded quickly under acidic and alkaline pH conditions ( $t_{1/2}$  1.6 days at pH 3, and 2.4 days at pH 9) with slower degradation rates observed at pH 5 and 7 (26 and 34 days, respectively). The latter two monobactams were then compared to the penam amoxicillin. The degradation kinetics of amoxicillin was different under all pH conditions; however, it was still on a timescale similar to the monobactams, with the longest  $t_{1/2}$  of 46 days at pH 5 and the fastest  $t_{1/2}$  of 6 days at pH 3.4 These aforementioned studies thus indicated that the degradation kinetics of  $\beta$ -lactam antibiotics was dependent on both the compound structure and the pH conditions. These prior studies mostly followed the disappearance of the parent antibiotic compound; little is known about the structural characteristics of the degradation compounds. 16,24,25

In addition to acid—base chemistry and the compound structure, the presence of metal ions, 16,17,26–32 minerals, 18 and organic matter<sup>17</sup> in surface waters is expected to influence the fate of  $\beta$ -lactam antibiotics. For example, previous studies have shown that Zn(II), <sup>28</sup> Cu(II), <sup>16,17,27,29,32</sup> Co(II), <sup>27</sup> Mn(II), <sup>30</sup> and Fe(III)<sup>26,31</sup> ions can promote hydrolysis of  $\beta$ -lactam antibiotics, as well as that the redox properties of the metal ion can promote oxidation of parent and transformation product compounds. Furthermore,  $\beta$ -lactam antibiotics have been shown to adsorb to soil particles, including clays. 15,33-35 Adsorption to clay particles has been considered for  $\beta$ -lactam removal from wastewater solution. <sup>33,34</sup> Other antibiotic classes such as sulfonamides, <sup>36–41</sup> tetracyclines, <sup>42–47</sup> and fluoroquinolones, 48-52 have been well studied with respect to their mechanisms of adsorption and degradation. However, mechanistic studies on interactions of  $\beta$ -lactam antibiotics with environmental adsorbents are lacking.9 A recent theoretical study of the adsorption mechanisms of two penam antibiotics, ampicillin and amoxicillin, on the clay vermiculite revealed the importance of Mg $-\pi$  interactions and interactions between Mg of the mineral and electronegative atoms (S and O) of the antibiotic.35 The mechanisms of interaction for different classes of  $\beta$ -lactam antibiotics with mineral surfaces remain to be investigated.

Here, using both experimental and theoretical approaches, we seek to investigate the fate of four  $\beta$ -lactam antibiotics (two penams: amoxicillin and cloxacillin; two cephems: cephalexin and ceftriaxone) under different aqueous conditions at pH 5.0 and pH 7.0. Figure 1 illustrates the structures of the four investigated  $\beta$ -lactam antibiotics and their reported acid—base chemistry. 53-56 First, we measured the stability of the parent compound with respect to hydrolysis in water. Second, we characterized hydrolysis byproducts using high-performance liquid chromatography (HPLC) coupled with ultraviolet (UV) detection or high-resolution mass spectrometry (MS). Passage through the LC column allows for the separation of compounds based on their polarity and affinity to the column, followed by further structure elucidation based on light absorption at different wavelengths using UV detection or based on specific mass after ionization using MS. Third, the mechanisms of interaction of the  $\beta$ -lactam antibiotics with a common smectite-type clay mineral, montmorillonite, were studied using X-ray diffraction (XRD), Fourier-transform

infrared spectroscopy (FTIR), and molecular modeling simulations. The XRD patterns probed the intercalation of the antibiotic compounds within the clay interlayer nanopores, the FTIR analysis was to capture vibration bands associated with specific functional groups involved in the antibiotic adsorption, and the molecular modeling simulations generated thermodynamically favorable adsorbate conformations to study mechanisms of interactions at the water-clay interface. Fourth, given the ubiquitous presence of dissolved organic matter (DOM) in surface waters, we probed the influence of different concentrations of a DOM on the mineral-mediated removal of the antibiotics from solution. The findings from this study provide new insights on the factors that can control the fate of the different compound structures within the  $\beta$ -lactam class of antibiotics in environmental aqueous media such as rivers, lakes, and at the water-sediment interface.

#### 2. EXPERIMENTAL AND COMPUTATIONAL SECTIONS

Further details on the experimental methods, instrument acquisition parameters, and molecular modeling setup are provided in Appendix A, Supporting Information.

**2.1. Materials.** The  $\beta$ -lactam antibiotics, amoxicillin (#A8523), cephalexin (#C4895), ceftriaxone (#C5793), and cloxacillin (#C9393), were purchased from Sigma-Aldrich (St. Louis, MO). Wyoming sodium montmorillonite (SWy-2) was purchased from the Clay Mineral Society (West Lafayette, IN) and has the reported structure of (Ca<sub>0.12</sub>Na<sub>0.32</sub>K<sub>0.05</sub>)[Al<sub>3.01</sub>Fe- $(III)_{0.41}Mn_{0.01}Mg_{0.54}Ti_{0.02}][Si_{7.98}Al_{0.02}]O_{20}(OH)_{4} \quad (octahedral$ charge -0.53; tetrahedral charge -0.02). The DOM sample used was Pahokee peat humic acid (#1S103H) obtained from the International Humic Substances Society. Solutions were prepared using purified deionized water (18.2 M $\Omega$  cm; MilliQ Advantage A10). Other chemicals used are listed in Appendix A, Supporting Information. All chemicals, including montmorillonite and Pahokee peat humic acid, were used as received without further purification.

2.2. Hydrolysis and Adsorption Experiments. We monitored the hydrolysis and adsorption of two penam (amoxicillin and cloxacillin) and two cephem (cephalexin and ceftriaxone)  $\beta$ -lactam antibiotics onto montmorillonite clay (0.5 g L<sup>-1</sup>). For all experiments conducted in this study (unless stated otherwise), the background solution comprised 10 mM NaCl, 10 mM sodium acetate, and 10 mM sodium bicarbonate; the solution was adjusted either to pH 5.0 or pH 7.0 with small aliquots of either 1 N NaOH or HCl. The detailed experimental setup is provided in Appendix A (Supporting Information).

Kinetic experiments were conducted at an initial  $\beta$ -lactam concentration of 50  $\mu$ M and provided two sources of information. First, the controls allowed us to monitor the extent of hydrolysis in our buffered background solution in the absence of montmorillonite by following the decrease in parent compound concentration. Second, the samples provided the equilibration time required for each antibiotic to adsorb to the montmorillonite (9 days for amoxicillin and cephalexin, 12 days for ceftriaxone). Amoxicillin, cloxacillin, and cephalexin were run with independent duplicates and one control, whereas ceftriaxone had independent triplicates and two controls. Kinetic experiments were sampled daily for up to 12 days when all the samples had reached equilibrium.

Adsorption isotherm experiments were produced for the  $\beta$ lactam compounds that exhibited an affinity for the montmorillonite surface in the kinetic experiments. The initial

loading of  $\beta$ -lactam antibiotic ranged from 0 to 500  $\mu$ M. For amoxicillin and cephalexin, samples were mixed for 9 days before analysis, whereas ceftriaxone was allowed 12 days to equilibrate based on the abovementioned study of time to reach equilibrium. All adsorption isotherm experiments were conducted with independent triplicates.

Finally, the DOM sample (final DOM concentration: 0, 10 or 100 mg L<sup>-1</sup>) was added to two solutions of ceftriaxone or amoxicillin (50 or 125  $\mu$ M) prepared in the aforementioned background buffer matrix and adjusted to pH 7.0. We added the DOM-containing antibiotic solution to 20 mg of montmorillonite (0.5 g L-1) and equilibrated for 12 days (independent triplicates).

2.3. Solution Analysis of  $\beta$ -Lactams and Hydrolysis Products. Several methods have been used previously to analyze the  $\beta$ -lactams in solution, including HPLC with UVdiode array detection (DAD), <sup>2,4,7,57-59</sup> liquid chromatography–MS with electrospray ionization, <sup>4,5,7,57,60</sup> and isothermal microcalorimetry. 19 Here, we leveraged our access to multiple instruments to conduct different analyses of the hydrolysis products: HPLC coupled with either a single channel UV detector or DAD was used for the quantification of each parent  $\beta$ -lactam in solution in the kinetic and adsorption experiments; and both MS and HPLC coupled with DAD were used for the characterization of the parent compound and hydrolysis byproducts. Detailed parameters for the liquid chromatography are provided in Appendix A (Supporting Information).

To further characterize the observed hydrolysis products, two sets of 50  $\mu$ M samples (in triplicates) of each  $\beta$ -lactam were prepared in the experimental buffered solution matrix (pH 5.0 and pH 7.0) in the absence of clay. One set of samples was immediately frozen (to be used as a reference, t = 0 days) and the other set was shaken on an orbital table (150 rpm) in an incubator (25 °C) for 12 days (t = 12 days) prior to HPLC-DAD analysis after sample filtering (0.2  $\mu$ m nylon). The resulting chromatograms were analyzed for the evolution of new peaks in the 3D-DAD data (190-400 nm scan range). A representative spectrum was extracted for the parent compound from the reference sample (t = 0 days) and a corresponding spectrum from the 12-day sample for potential hydrolysis products. For the analysis of hydrolysis products with high-resolution MS, we prepared equivalent samples in a water background solution (without salts) as high concentrations of (nonvolatile) salt solutions can cause precipitation on the MS hardware and ionization suppression (or decreased sensitivity). 61,62 Details on the mass spectrometer parameters and the MS analysis are provided in Appendix A (Supporting Information).

2.4. XRD and FTIR Measurements. We used XRD and FTIR spectroscopy to analyze the montmorillonite clay complexes with the  $\beta$ -lactam antibiotic. Samples of amoxicillin, cephalexin, or ceftriaxone with montmorillonite at pH 7 were prepared for XRD analysis using the same procedure outlined for kinetic and adsorption experiments at initial antibiotic loading concentrations ranging from 0 to 500 µM. After centrifugation, the supernatant was discarded, and the resulting clay slurry was refrigerated until XRD analysis. For sample preparation, the antibiotic-montmorillonite slurry was pipetted onto a flat XRD sample holder and first allowed to air-dry before being equilibrated in the XRD sample chamber at 15-20% relative humidity and ~25 °C.

Samples for FTIR measurements were prepared in the absence of acetate and bicarbonate buffer to avoid spectral

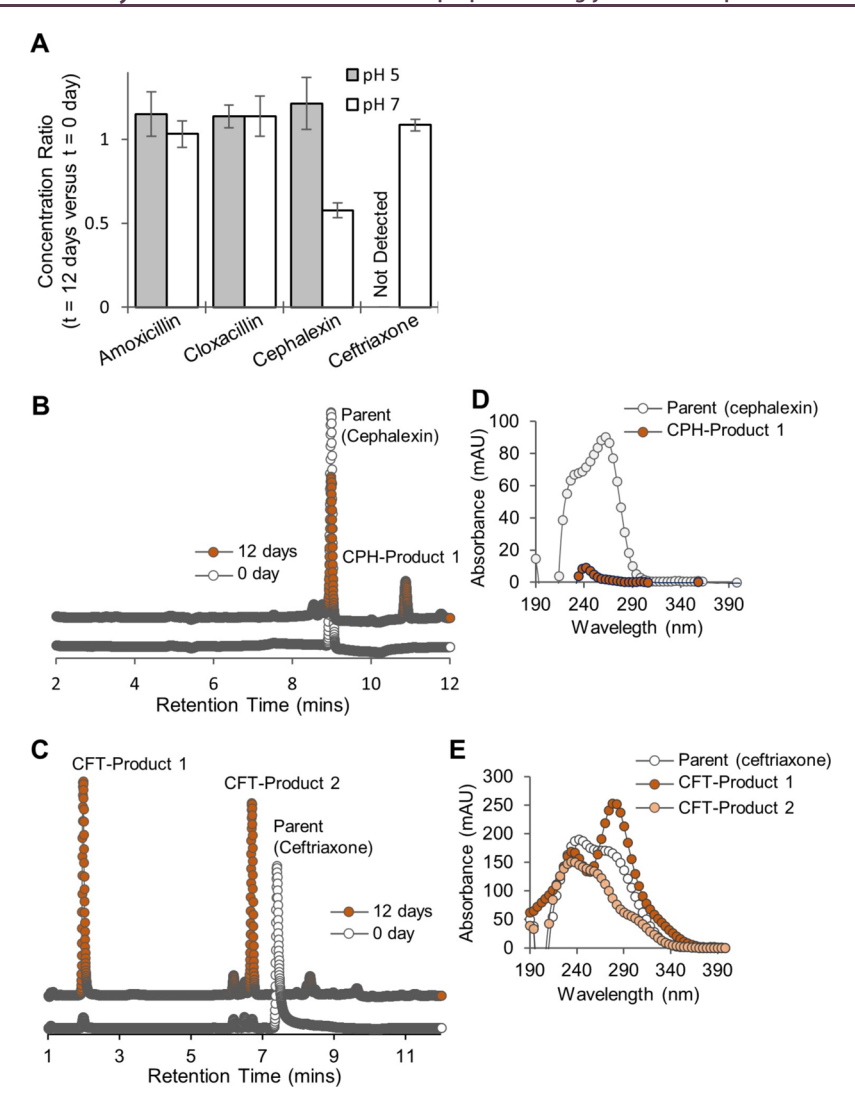


**Figure 2.** Characterizing hydrolysis of the β-lactam antibiotics in buffered solution at pH 5.0 and pH 7.0. (A) Fractional amount of antibiotic remaining in solution after 12 days: pH 5.0 (gray bars); pH 7.0 (white bars). Error bars represent one standard deviation (n = 3). (B,C) Representative chromatograms acquired at λ = 240 nm of cephalexin equilibrated at pH 7.0 (B) and ceftriaxone equilibrated at pH 5.0 (C). White filled circles = 0 days, red filled circles = 12 days. Chromatograms are offset for display purposes. (D) Extracted spectra from the 3D-DAD data of the cephalexin parent compound (retention time = 8.97 min) and a new peak at 10.87 min (CPH-Product 1) observed in the 12 days pH 7.0 sample. (E) Extracted spectra from the 3D-DAD data of the ceftriaxone parent compound (retention time = 7.40 min) and the two new peaks observed at 1.98 min (CFT-Product 1) and 6.70 min (CFT-Product 2) in the 12 days pH 5.0 sample.

interferences from these compounds. The NaCl concentration was increased to 30 mM to maintain ionic strength. Samples (in triplicates) of amoxicillin, cephalexin, and ceftriaxone (each at 250  $\mu\rm M$  and adjusted to pH 7.0 using small aliquots of either NaOH or HCl) were prepared with montmorillonite (0.5 g  $\rm L^{-1}$ ) and equilibrated for 11 days on an incubated orbital table at 150 rpm and 25 °C. The samples were then centrifuged at 2000 g for 20 min and the supernatant retained for HPLC analysis. The resulting clay pellets were lyophilized immediately, and the dried samples were homogenized using an agate mortar and pestle in preparation for FTIR analysis. Details on the instrument parameters for the XRD and FTIR analyses are provided in Appendix A (Supporting Information).

**2.5. Molecular Modeling Simulations.** We simulated adsorbate conformations of amoxicillin (a penam) and cephalexin (a cephem) on montmorillonite, using Biovia's Materials Studio and Discovery Studio software packages. <sup>63,64</sup> To account for the ionization scheme of the antibiotics across the pH values of the adsorption experiments (pH 5.0 and 7.0)

(Figure 1A,C), we performed the simulations with zwitterionic amoxicillin, zwitterionic cephalexin, and negatively charged cephalexin. The condensed-phase optimized molecular potentials for atomistic simulation studies (COMPASS) forcefield (version II) has previously been shown to be effective in modeling the interactions between montmorillonite clay and antibiotics. 45,65

To ensure that the structural conformations provided by the molecular modeling approach used here agree with experimentally derived data, we conducted validation analyses by comparing the simulated structural data with experimentally obtained X-ray crystallography data for amoxicillin and cephalexin. Details on how the validation simulations were conducted are provided in Appendix A (Supporting Information). Within an error imprecision of two standard deviation values, we obtained good agreement between the experimental and simulated data: 92% of the bond lengths and 83% of the angle measurements for amoxicillin 66 and 89% of

the bond lengths and 79% for cephalexin (Supporting Information, Appendix B and C).<sup>67</sup>

For the adsorption simulations, the basal clay surfaces of a Wyoming-type montmorillonite were prepared as done previously,<sup>68</sup> with an average stoichiometry of Na<sub>0.2</sub>(Si<sub>8</sub>) (Al<sub>3.5</sub>Mg<sub>0.5</sub>)O<sub>20</sub>(OH)<sub>4</sub> for a unit cell subjected to periodic extension to obtain a  $42.24 \times 36.56 \times 45.00 (x \times y \times z) \text{ Å}^3$ supercell. This supercell contained a total charge of -16 due to random isomorphic substitutions of Al<sup>3+</sup> to Mg<sup>2+</sup> throughout the octahedral sheet. Details on how the solvent with explicit water molecules was prepared are provided in Appendix A (Supporting Information). We used the Monte Carlo search approach via the Adsorption Locator module of Materials Studio and the COMPASS forcefield to obtain energy- and geometry-optimized adsorbate conformations for the adsorption of zwitterionic amoxicillin, zwitterionic cephalexin, and negatively charged cephalexin on the montmorillonite surface. 45,65,69 Details on how the Monte Carlo yielded thermodynamically favorable hydrated antibiotic-clay complexes are provided in Appendix A (Supporting Information). The configurations were analyzed for hydrogen bonding (direct and water-bridged) interactions and close contacts between the antibiotic compound or Na+ and the clay surface or surrounding hydrated waters. A maximum H-donor distance of 3 Å and minimum donor-H-acceptor angle of 120° was used; a close contact cutoff of 2.5 Å was used. 69,70

#### 3. RESULTS

3.1. pH Dependence and Compound Dependence of  $\beta$ -Lactam Hydrolysis. Due to the reported hydrolysis of  $\beta$ lactams, we first performed 12-day kinetic experiments to probe the stability of the different  $\beta$ -lactam compounds in the solution buffered at pH 5.0 or pH 7.0. Linear regression of the control samples indicated that both penams and cephems follow a pseudo-first-order rate of hydrolysis (Supporting Information, Appendix D). Only the cephems (ceftriaxone at pH 5.0 and cephalexin at pH 7.0) were found to disappear from solution at a rate fast enough ( $t_{1/2}$  of 2.4 days and 12 days, respectively) to be significant on the timescale of this study. The observed decline was confirmed in a separate experiment by comparing the concentration of the parent antibiotic compound after 12 days equilibration versus freshly prepared in the buffered solution. After 12 days in the buffer solution, ceftriaxone was no longer present when equilibrated at pH 5.0 and only 50% of cephalexin remained in solution at pH 7.0 (Figure 2A).

The evolution of new products due to the occurrence of hydrolysis (or lack thereof) was first confirmed by analysis of the four compounds in buffer solution after 0 days (reference) and 12 days equilibration using HPLC with UV detection (Supporting Information, Appendix E). Here, we focused on the data for the systems that were likely to undergo hydrolysis due to the disappearance of the parent compounds in solution, as previously discussed. For cephalexin at pH 7.0, the parent compound had a retention time at 8.98 min, and after 12 days, there was a decrease in the peak associated with the parent compound and a new peak at 10.85 min (CPH-Product 1) in the chromatogram emerged (Figure 2B). For ceftriaxone at pH 5.0, the peak at 7.40 min associated with the parent compound was absent after 12 days, and two new peaks appeared at 1.98 min (CFT-Product 1) and 6.70 min (CFT-Product 2) in the chromatogram (Figure 2C).

Using DAD data, we further examined the spectrophotometric profiles of the new peaks (hydrolysis products) compared to their respective parent compound (Figure 2D,E). Cephalexin had an absorption maximum at 265 nm, which was absent in the extracted spectrum for CPH-Product 1—the apparent maximum at approximately 230–240 nm might be an artifact due to the strong negative absorption band below 220 nm caused by methanol in the chromatography gradient (Figure 2D). The spectrum of CPH-Product 1 implied that the hydrolysis product was devoid of the conjugated benzene and cephem moieties, which would be responsible for the 265 nm band in the parent compound. 72,73

With respect to ceftriaxone at pH 5.0, the spectrum for the parent compound aligned with that previously reported for ceftriaxone, 74 with a distinct maximum at 238 nm and a broad maximum at ~280 nm (Figure 2E). For the ceftriaxone hydrolysis products, we found that CFT-Product 1 had two distinct maxima at 234 and 280 nm, and a small shoulder at ~335 nm (Figure 2E). The CFT-Product 1 likely did not possess the cephem functional group with the  $\beta$ -lactam ring due to the absence of a peak at 264 nm. 73 A reportedly common stable hydrolysis product of ceftriaxone is thiotriazinone (2-methyl-3-sulfanyl-1,2-dihydro-1,2,4-triazine-5,6-dione, also known as Ceftriaxone EP Impurity C), which is the sixmembered ring with the attached sulfhydryl group (Figure 1D). 24,75,76 Two maxima at 222 nm and 271 nm were reported in the thiotriazinone spectrum,<sup>75</sup> wherein the latter peak (271 nm) was shown to have a stronger absorbance than the peak at 222 nm, which aligned with the observed UV-absorption profile of CFT-Product 1 (Figure 2E). Therefore, we proposed that the extracted spectrum of CFT-Product 1 was from thiotriazinone, despite the spectrum being bathochromatically shifted by ~10 nm compared with the spectrum reported previously (Figure 2E)<sup>75</sup>—this proposal was further validated by MS analysis as discussed below. The spectrum for CFT-Product 2 had three maxima at ~235 nm (obscured by the negative methanol absorbance), 263 nm, and 305 nm (Figure 2E). Previous work has shown adsorption bands associated with substructures of ceftriaxone at maxima of 270 nm for the 2-aminothiazole (5-membered ring) moiety<sup>77</sup> and at 240, 256, and 270 nm for the 7-aminocephalosporanic acid functional group (cephem functional group).<sup>72</sup> Moreover, using LC-MS analysis, the remaining structure of ceftriaxone (minus the thiotriazinone ring; (6R,7R)-7-[[(2Z)-2-(2-amino-4-thiazolyl)-2-(methoxyimino)acetyl]amino]-3-(hydroxymethyl)-8-oxo-5thia-1-azabicyclo [4.2.0] oct-2-ene-2-carboxylic acid, or 3-desacetyl cefotaxime also known as Cefotaxime Impurity B) was previously identified as the second product of hydrolysis.<sup>76</sup> Therefore, after the thiotriazinone ring has been cleaved, we assumed that the remaining structure (3-desacetyl cefotaxime) can be attributed to CFT-Product 2.

To obtain additional insights into the hydrolysis products and to confirm our predictions from the chromatographic and spectrophotometric analyses, we performed MS analysis using direct infusion. Due to the nonvolatile salts used in the eluents of the HPLC-UV chromatography, we could not easily apply the HPLC-UV chromatography method in a LC-MS method; hence, the direct infusion approach was chosen. First, we conducted a comparative analysis of the extent of hydrolysis for each compound in the water background versus the salt-containing buffered solution (Supporting Information, Appendix F). The extent of hydrolysis (relative to control) for the penams revealed that these compound structures were slightly

Scheme 1. Hydrolysis Products of Ceftriaxone at pH 5.0<sup>a</sup>

"Shown are the neutral parent compound and the two dominant product ions, thiotriazinone and 3-desacetyl cefotaxime, determined by mass spectrometry. The identified adducts associated with the hydrolysis products are shown in the superscript texts.

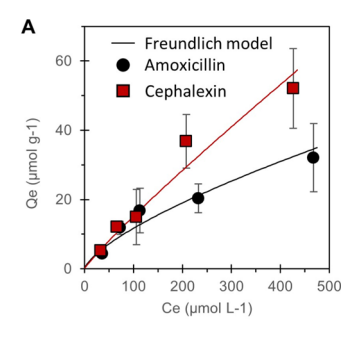
more stable in the buffered solution than in the unbuffered solutions [amoxicillin:  $1.15 \pm 0.13$  (buffer) versus  $0.89 \pm 0.02$ (water) at pH 5.0 (p < 0.001), and 1.03  $\pm$  0.08 (buffer) versus  $0.95 \pm 0.01$  (water) at pH 7.0 (p < 0.001); cloxacillin: 1.14  $\pm$ 0.07 (buffer) versus  $0.88 \pm 0.02$  (water) at pH 5.0 (p < 0.001), and  $1.14 \pm 0.12$  (buffer) versus  $0.92 \pm 0.03$  (water) at pH 7.0 (p < 0.001)] (Supporting Information, Appendix F). The corresponding data for the cephems revealed variable extent of hydrolysis for the cephems depending on solution pH [cephalexin:  $1.12 \pm 0.15$  (buffer) versus  $0.89 \pm 0.01$  (water) at pH 5.0 (p < 0.001), and 0.58  $\pm$  0.04 (buffer) versus 0.89  $\pm$ 0.01 (water) at pH 7.0 (p < 0.001); ceftriaxone: complete hydrolysis at pH 5.0, and 1.09  $\pm$  0.04 versus 0.29  $\pm$  0.01 (water) at pH 7.0 (p < 0.001)] (Supporting Information, Appendix F). Notably, there was considerably less hydrolysis for cephalexin in the water background at pH 7 compared with the buffered solution, and hydrolysis of ceftriaxone at pH 5 was enhanced by 80% in the water background (Supporting Information, Appendix F). We attributed the change in the stability of the cephems to pH drift in the unbuffered water (Supporting Information, Appendix F). Nevertheless, it could be possible to detect hydrolysis products for cephalexin at low concentrations using MS, depending on the ionization ability of the hydrolysis fragment.

We obtained mass spectra for all four  $\beta$ -lactam antibiotics in both positive and negative ionization modes at both pH 5.0 and 7.0 (Supporting Information, Appendix G). Signal intensities in positive ionization mode were 1-3 orders of magnitude greater than the intensities in the negative ionization mode (Supporting Information, Appendix G). Supporting the kinetic experiment results and HPLC-UV analysis, the MS results did not show any unknown ions at significant abundance for both penams, amoxicillin or cloxacillin, at either pH (Supporting Information, Appendix H). For cephalexin (pH 7.0) where hydrolysis was expected, the reference spectra (0 days) showed common adducts with the parent compound to produce positive ions  $([M + H]^+, [M$ + K]<sup>+</sup>, [2M + H]<sup>+</sup>, and [M + Na]<sup>+</sup>) and negative ions ([M + K]) Cl] $^{-}$ ,  $[2M - H]^{-}$ , and  $[M - H]^{-}$ ). After 12 days in the solution, the MS data did not detect any new identifiable unknown ions or likely hydrolysis products (Supporting Information, Appendix H). We attributed this result to the pH drift of the unbuffered solution, which resulted in a final pH of 5.6.

With respect to ceftriaxone (pH 5.0), common adducts with the parent compound were present in the reference spectra to produce the negative ions  $[M-H]^-$ ,  $[M-2H]^{2-}$ , and  $[M+Na-2H]^-$  and the positive ions  $[M+Na]^+$ ,  $[M+2Na]^{2+}$ ,  $[M+H]^+$ ,  $[M+Na+H]^{2+}$ ,  $[M+K]^+$ , and  $[M+2Na-H]^+$  (Supporting Information, Appendix H). Furthermore, in the

reference spectra in negative ionization mode, three unknown ions were measured that could be attributed to part of the ceftriaxone structure: m/z = 158.0018 ( $C_4\bar{H}_4O_2N_3S^-$ ; Ceftriaxone EP Impurity C; the thiotriazinone ring), m/z =394.0285 (C<sub>14</sub>H<sub>12</sub>O<sub>5</sub>N<sub>5</sub>S<sub>2</sub><sup>-</sup>; Ceftriaxone EP Impurity B), and  $m/z = 350.0389 (C_{13}H_{12}O_3N_5S_2^-; Impurity B-[CO_2])$ (Supporting Information, Appendix H). It was not possible to resolve the structural arrangement of the m/z = 350.0389ion. After 12 days in the solution, no known parent ions for ceftriaxone were observed in the top 20 ions exported from the MS spectra for either positive or negative ionization modes (Supporting Information, Appendix H). In negative ionization mode, two dominant hydrolysis products were identified: the aforementioned thiotriazinone ion (m/z = 158.0018;C<sub>4</sub>H<sub>4</sub>O<sub>2</sub>N<sub>3</sub>S<sup>-</sup>) and the product ion 3-desacetyl cefotaxime  $(m/z 412.0395; C_{14}H_{14}O_6N_5S_2^-)$  from the hydrolysis of the S-C bond to cleave the thiotriazinone ring (Supporting Information, Appendix H) (Scheme 1).<sup>76</sup> In positive ionization mode, we did not observe the thiotrazinone ion, but four ions associated with 3-desacetyl cefotaxime were dominant: a proton adduct (C<sub>14</sub>H<sub>16</sub>O<sub>6</sub>N<sub>5</sub>S<sub>2</sub><sup>+</sup>), a sodium adduct (C<sub>14</sub>H<sub>15</sub>O<sub>6</sub>N<sub>5</sub>S<sub>2</sub>Na<sup>+</sup>), a double sodium adduct (C<sub>14</sub>H<sub>15</sub>O<sub>6</sub>N<sub>5</sub>S<sub>2</sub>Na<sub>2</sub><sup>2+</sup>), and a potassium adduct  $(C_{14}H_{15}O_6N_5S_2K^+)$  (Supporting Information, Appendix H) (Scheme 1). Positive ionization recorded one additional ion of significance, m/z = 261.0652, which we assigned the stoichiometry composition C<sub>8</sub>H<sub>13</sub>O<sub>4</sub>N<sub>4</sub>S<sup>+</sup> based on the natural isotope signature (Supporting Information, Appendix H). Taken collectively, we concluded that CFT-Product 1 identified in the HPLC-UV analysis is the thiotriazinone moiety (Figure 2E). 24,75 Thus, CFT-Product 2 was likely the remaining cleaved fragment of ceftriaxone, 3-desacetyl cefotaxime, given the high ion abundance in the m/z spectrum.

3.2. pH-Dependent Extent of Adsorption on a Smectite Clay Mineral and Influence of Organic Matter. We obtained adsorption isotherms, with initial concentrations up to 500  $\mu$ mol L<sup>-1</sup>, for the  $\beta$ -lactam compounds at the pH conditions wherein there was minimal to no hydrolysis: amoxicillin and cephalexin at pH 5.0; amoxicillin, cephalexin, and ceftriaxone at pH 7.0 (Figure 3). Our reported quantified amount of antibiotics adsorbed on the montmorillonite clay accounted for the occurrence of hydrolysis, especially in the case of cephalexin. The adsorption results were fitted with a Freundlich isotherm model (full modeling parameters are listed in the Supporting Information, Appendix I). At pH 5.0, the highest amount adsorbed for amoxicillin and cephalexin was found to be 32 and 52  $\mu$ mol g<sup>-1</sup>, respectively (Figure 3A). At a relatively higher pH value (pH 7.0), the adsorption capacity reached 294, 218, and 116  $\mu$ mol g<sup>-1</sup> of amoxicillin, cephalexin, and ceftriaxone, respectively (Figure 3B). Under



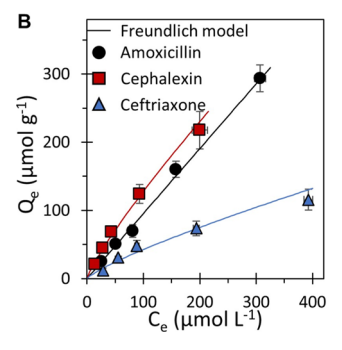


Figure 3. Adsorption isotherms fitted with a Freundlich model. (A) Adsorption isotherms generated at pH 5.0 for amoxicillin (black circles) and cephalexin (red squares) in the experimental buffer solution. (B) Adsorption isotherms generated at pH 7.0 for amoxicillin (black circles), cephalexin (red squares), and ceftriaxone (blue triangles). Initial concentrations ranged from 0 to 500  $\mu$ M. Error bars represent one standard deviation (n = 3) in both x- and ydirections. Where error bars are not visible, the symbol is larger than

our experimental conditions, a fourfold increase in adsorption occurred when the pH was increased from 5.0 to 7.0 (Figure 3). For example, an initial solution concentration  $(C_0)$  of 125  $\mu M$  of amoxicillin resulted in 17  $\mu mol g^{-1}$  of amoxicillin adsorbed onto montmorillonite at pH 5.0 compared to 70  $\mu$ mol g<sup>-1</sup> at pH 7.0 (Figure 3). Similarly, a  $C_0$  of 125  $\mu$ M of cephalexin resulted in adsorbed amounts of 15 and 69  $\mu$ mol g<sup>-1</sup> at pH 5.0 and 7.0, respectively (Figure 3).

To evaluate the influence of DOM on the extent of antibiotic adsorption at pH 7.0, we reacted amoxicillin and ceftriaxone with the clay in the presence of an increasing concentration of a DOM isolate (a peat humic acid). Here, we monitored the fractional amount of the initial antibiotic amount that remained in solution (i.e., not adsorbed on the clay) because our solution analysis was not able to distinguish between the antibiotic being removed from solution through complexation by DOM, adsorption to the clay, or both. Therefore, our data provided insights only on how DOM interfered with the removal of free antibiotic in solution. In the absence of DOM, approximately 50% of the amoxicillin parent compound remained free in solution and 50% was adsorbed to the montmorillonite clay [irrespective of the initial antibiotic concentration (50 or 125  $\mu$ M) (Figure 4A). The presence of DOM (10 or 100 mg L<sup>-1</sup>) had minimal effect on the fractional amoxicillin concentration in solution (51 to 59%) compared to when the DOM was absent (50%) (Figure 4A). In contrast, the presence of the DOM interfered with the removal of ceftriaxone from solution (Figure 4B). Specifically, when 10 mg L<sup>-1</sup> of DOM was added to the system, it increased the fractional concentration of free ceftriaxone in solution to 85%, compared to  $\sim$ 70% in the absence of DOM (Figure 4B).

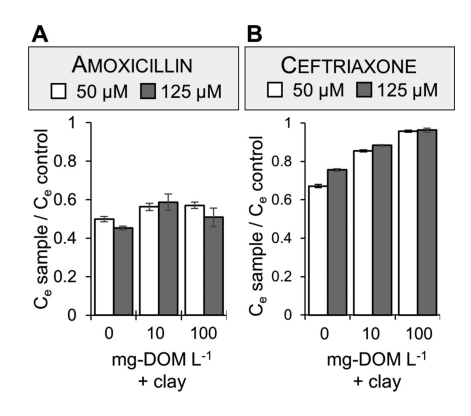


Figure 4. Ratio of remaining amoxicillin (A) and ceftriaxone (B) in solution following a 12-day reaction with the clay (montmorillonite) at pH 7.0 in the presence of 0, 10, or 100 mg L<sup>-1</sup> DOM (as Pahokee peat humic acid). The reactions were conducted with two initial solution concentrations of the antibiotics: 50  $\mu$ M (white bars) and 125 µM (gray bars). The appropriate control experiment contained the initial antibiotic concentration in buffered solution without montmorillonite or DOM). Error bars represent one standard deviation (n = 3).

Furthermore, increasing the concentration of DOM to 100 mg  $L^{-1}$  further inhibited the removal of ceftriaxone from solution, where nearly all (~96%) of the ceftriaxone remained in solution (Figure 4B).

To gain insights into the adsorption mechanisms on the clay mineral, we conducted both XRD and FTIR analysis using antibiotic-clay samples under the pH condition (pH 7.0) wherein adsorption was the highest (Figure 5; Supporting Information Appendix J). Interlayer adsorption of antibiotics within montmorillonite matrices was monitored by a shift in the  $d_{001}$  peak position along the  $2\theta$  axis; this peak position is used to determine interlayer spacing via Bragg's law. 42-45,48-50 In addition, at low amounts of intercalated antibiotics,

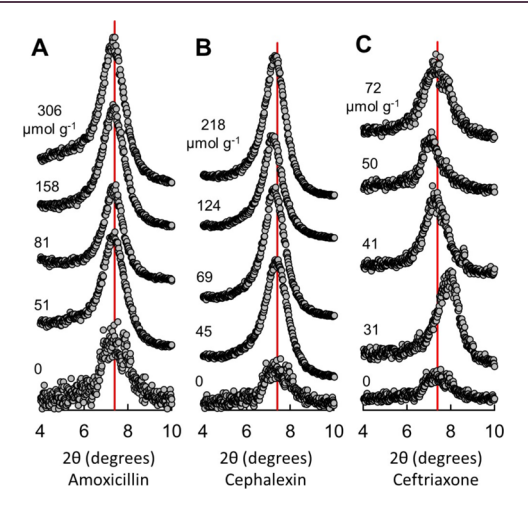


Figure 5. XRD patterns of (A) amoxicillin-montmorillonite, (B) cephalexin-montmorillonite, and (C) ceftriaxone-montmorillonite samples. The numbers on the left side of each XRD spectrum indicate the equilibrium amounts of adsorbed antibiotics (in  $\mu$ mol g<sup>-1</sup> clay). In A, from top to bottom, 306, 158, 81, 51, and 0  $\mu$ mol amoxicillin  $g^{-1}$  clay. In B, from top to bottom, 218, 124, 69, and 0  $\mu$ mol cephalexin g<sup>-1</sup> clay. In C, from top to bottom, 72, 50, 41, 31, and 0  $\mu$ mol ceftriaxone g<sup>-1</sup> clay. The red vertical line in each spectrum indicates the location of the  $d_{001}$  peak.

Table 1. Results from Adsorption Experiments and Experimental XRD Patterns of Montmorillonite Reacted with Amoxicillin and Cephalexin<sup>a</sup>

	amoxicillin				cephalexin				ceftriaxone			
initial concentration $(\mu \text{mol g}^{-1})$	amount adsorbed (µmol g <sup>-1</sup> )	d <sub>001</sub> (nm)	$\Delta d$	fwhm $(2\theta)$	amount adsorbed (µmol g <sup>-1</sup> )	d <sub>001</sub> (nm)	Δd	fwhm $(2\theta)$	amount adsorbed $(\mu \text{mol g}^{-1})$	d <sub>001</sub> (nm)	Δd	fwhm $(2\theta)$
0	0	1.19		1.49	0	1.19		1.49	0	1.19		1.49
80	51	1.21	0.02	0.96	45	1.21	0.02	1.05	31	1.12	0.07	1.17
125	81	1.21	0.02	0.87	69	1.22	0.03	0.97	41	1.21	0.02	1.22
250	158	1.21	0.02	0.98	124	1.23	0.04	0.84	50	1.22	0.03	0.92
500	306	1.21	0.02	0.97	218	1.21	0.02	0.98	72	1.20	0.01	1.47

 $<sup>^{</sup>a}d_{001}$ , the basal spacing between the clay layers;  $\Delta d$ , difference in interlayer spacing in the presence of adsorbed antibiotics relative to the montmorillonite alone; fwhm, full width at half-maximum intensity.

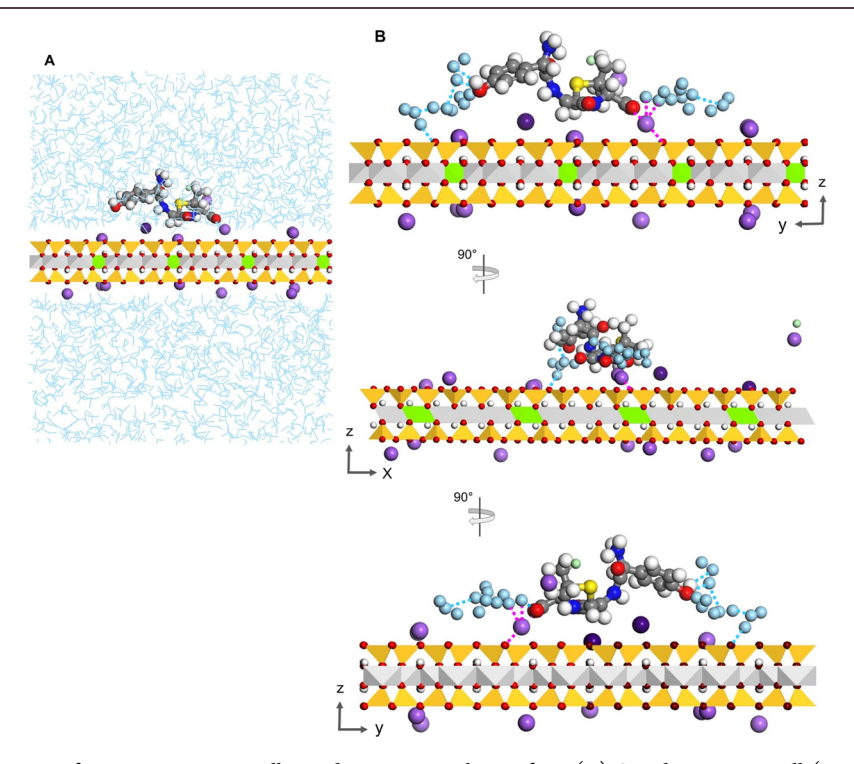


Figure 6. Molecular simulations of zwitterionic amoxicillin with a smectite clay surface. (A) Simulation supercell  $(42.24 \times 36.56 \times 45.00 \text{ Å}^3)$  of optimized antibiotic compound (zwitterionic amoxicillin) adsorbed on the basal surface of a model montmorillonite surface. (B) Close-up views of amoxicillin's interactions with hydrated water molecules, Na<sup>+</sup> ions, and the clay surface. Hydrogen bond interactions are represented by light-blue dotted lines and contact O atoms for Na<sup>+</sup> complexation sphere are shown with pink dotted lines. In B, the water molecules that are not involved in water-bridging hydrogen bonds, direct hydrogen bonds, or Na<sup>+</sup> hydration were removed for clarity. Atom color codes: oxygen (red), hydrogen (white), nitrogen (blue), sulfur (yellow), chloride (green), and sodium (purple); the clay structure is visualized using polyhedrons: silicon (dark yellow), aluminum (gray), magnesium (bright green).

interlayer adsorption can be captured by an increase in full width at half-maximum (fwhm) (i.e., a broadening of the peak shape), which features interstratification of different interlayer sizes, presumably those with or without adsorbed antibiotics. Here, we obtained a small increase of up to 0.04 nm in the interlayer spacing ( $d_{001}$ ) of some antibiotic—clay samples relative to the montmorillonite clay alone; there was no conclusive trend in the fwhm values (Figure 4; Table 1). In sum, our XRD data indicated that the antibiotic intercalation was not significant, implying that the adsorbed antibiotics were primarily on the basal surfaces external to smectite interlayer stackings.

With respect to the FTIR data, all of the spectra exhibited the expected vibrational bands associated with the mineral, including stretching ( $\nu$ OH, 3400 cm<sup>-1</sup>) and bending ( $\delta$ OH, 1634 cm<sup>-1</sup>) vibrations of structural OH, stretching of the tetrahedral sheet ( $\nu$ Si-O-Si, 1000 cm<sup>-1</sup>), and bending

vibrations of the octahedral sheet ( $\delta Al_2OH$ , 916 cm<sup>-1</sup>;  $\delta AlMgOH$ , 844 cm<sup>-1</sup>) (Supporting Information, Appendix J). However, there were no new or shifted bands in the spectra of the antibiotic—clay samples compared to the clay control, likely due to an insufficient amount of the antibiotic adsorbed on the clay surface to obtain detectable FTIR signatures of the adsorbed antibiotic (Supporting Information, Appendix J). Therefore, we employed molecular modeling simulations as an alternative approach to probe the mechanisms of interactions of amoxicillin and cephalexin with the clay surface.

3.3. Molecular Modeling Simulations Predicted Specific Clay–Antibiotic Adsorbate Conformations. Using molecular modeling simulations based on a Monte Carlo approach, we probed the thermodynamically favorable structures of the adsorbate conformations obtained with zwitterionic or negatively charged  $\beta$ -lactams (zwitterionic

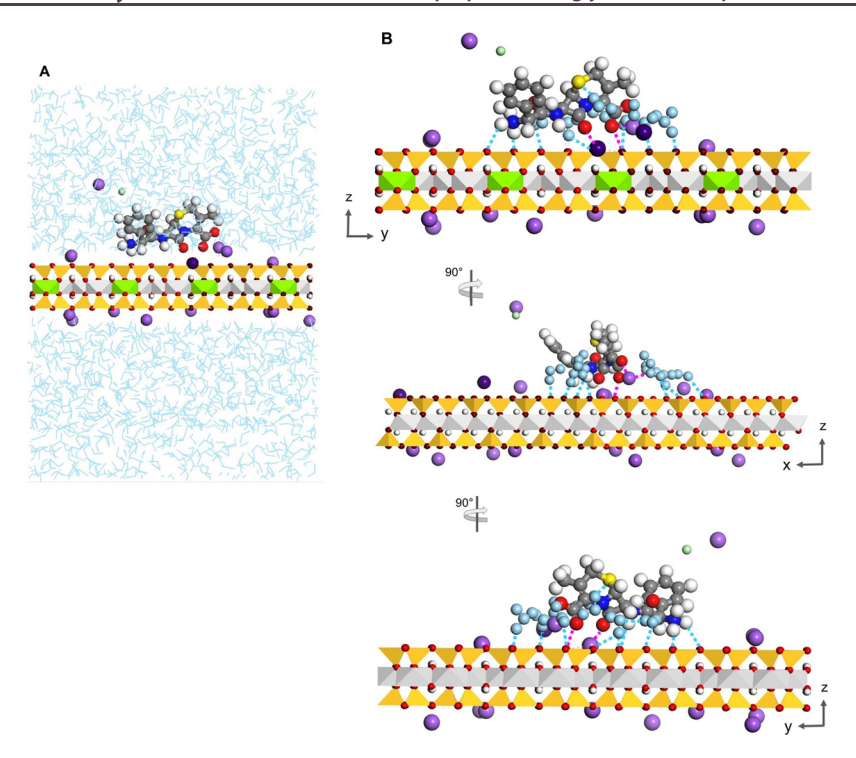


Figure 7. Molecular simulations of zwitterionic cephalexin with a smectite clay surface. (A) Simulation supercell  $(42.24 \times 36.56 \times 45.00 \text{ Å}^3)$  of optimized antibiotic compound (zwitterionic cephalexin) adsorbed on the basal surface of a model montmorillonite surface. (B) Close-up views of cephalexin's interactions with hydrated water molecules, Na<sup>+</sup> ions, and the clay surface. Hydrogen bond interactions are represented by light-blue dotted lines and contact O atoms for Na<sup>+</sup> complexation sphere are shown with pink dotted lines. In B, the water molecules that are not involved in water-bridging hydrogen bonds, direct hydrogen bonds, or Na<sup>+</sup> hydration were removed for clarity. Atom color codes: oxygen (red), hydrogen (white), nitrogen (blue), sulfur (yellow), chloride (green), and sodium (purple); the clay structure is visualized using polyhedrons: silicon (dark yellow), aluminum (gray), magnesium (bright green).

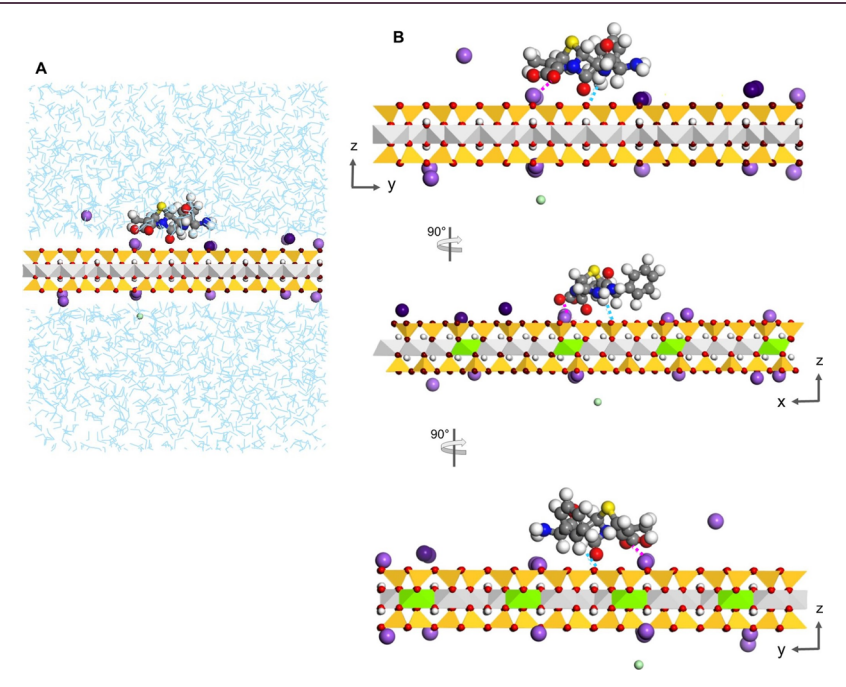


Figure 8. Molecular simulations of negatively-charged cephalexin with a smectite clay surface. (A) Simulation supercell  $(42.24 \times 36.56 \times 45.00 \text{ Å}^3)$  of optimized antibiotic compound (negatively-charged cephalexin) adsorbed on the basal surface of a model montmorillonite surface. (B) Close-up views of cephalexin's interactions with hydrated water molecules, Na<sup>+</sup> ions, and the clay surface. Hydrogen bond interactions are represented by light-blue dotted lines, and contact O atoms for Na<sup>+</sup> complexation sphere are shown with pink dotted lines. In B, the water molecules that are not involved in water-bridging hydrogen bonds, direct hydrogen bonds, or Na<sup>+</sup> hydration were removed for clarity. Atom color codes: oxygen (red), hydrogen (white), nitrogen (blue), sulfur (yellow), chloride (green), and sodium (purple); the clay structure is visualized using polyhedrons: silicon (dark yellow), aluminum (gray), magnesium (bright green).

amoxicillin, zwitterionic cephalexin, and negatively charged cephalexin) and the basal surface of a model Na-montmorillonite (Figures 6-8). A common feature in all three systems is the complexation of Na+ ions, already involved in innersphere complexation near a negatively charged site on the mineral surface by O atoms from hydrated water and the  $\beta$ lactam's carboxyl moiety (Figures 6–8). Notably, zwitterionic cephalexin also exhibited inner-sphere complexation with a second Na<sup>+</sup> ion, which was positioned vicinal to one of the clay's negatively charged sites (Figure 7B). Solvated water molecules around the zwitterionic amoxicillin and zwitterionic cephalexin compounds resulted in a water-bridged network of hydrogen bonds with the mineral surface (Figures 6B and 7B). Whereas the primary amine of the zwitterionic amoxicillin was positioned away from the clay surface, the phenol ring of the zwitterionic amoxicillin pointed directly toward the clay, which mediated one hydrogen bond to the montmorillonite surface (Figure 6B). By contrast, the primary and secondary amine moieties in both the zwitterionic and negatively charged cephalexin compounds were oriented in such a fashion to facilitate two or one direct hydrogen bonds with the clay surface, respectively (Figures 7B and 8B). In addition, the sulfur-containing moiety in zwitterionic cephalexin participated in a network of water-bridging interactions that anchored this cepham antibiotic to the clay surface via two hydrogen bonds (Figure 7B). Therefore, the conformational arrangement afforded by the cephem antibiotic structure promoted more favorable interactions with the mineral surface than the conformation of the penam antibiotic (Figures 6–8). In sum, based on the total intermolecular interactions predicted by the molecular simulations, the order of favorable conformations of the adsorbed antibiotics on the clay surface was as follows: zwitterionic cephalexin > zwitterionic amoxicillin > negatively charged cephalexin (Figures 7 and 8).

## 4. DISCUSSION

Understanding the factors that control the aquatic fate of  $\beta$ lactams, the class of antibiotics most used worldwide, is of special interest. 1,3,9,10 Given the presence of different generations of  $\beta$ -lactam antibiotics in wastewater and surface waters, it is important to investigate different structures of  $\beta$ -lactams. 5-7,10-12,14 The degradation kinetics of  $\beta$ -lactam antibiotics are known to depend highly on environmental conditions. 4,15,19,60 Moreover, antibiotics are expected to interact with mineral and organic particles, both of which can influence the extent of hydrolysis. 60 However, few studies have examined beyond the degradation of one parent compound into degradation products or investigated the underlying mechanisms of interactions of  $\beta$ -lactams with mineral surfaces. Here, using experimental and theoretical methods, we investigated the hydrolysis of structurally different  $\beta$ -lactam compounds in solution and probed the interactions of these compounds with minerals and the influence of the presence of DOM.

During the timespan of our experiments, significant degradation was only recorded for the cephem compounds, ceftriaxone at pH 5.0 and cephalexin at pH 7.0. Hydrolysis of ceftriaxone under similar abiotic experimental conditions has been shown previously, with  $t_{1/2}$  values ranging from 19.5 d at pH 6.0 to 21–103 d at pH 7.0. These  $t_{1/2}$  values for ceftriaxone at pH 6.0 and 7.0 are consistent with our data at pH 7.0 result ( $t_{1/2}$  64 d) but are substantially slower than what we measured for ceftriaxone at pH 5.0 ( $t_{1/2}$  2.4 d).

Interestingly, our observation of a faster hydrolysis rate for ceftriaxone at the acidic pH compared to the circumneutral pH seemed contradictory to previous studies, 16,20,22,31 which reported a base-catalyzed hydrolysis reaction for  $\beta$ -lactam antibiotics whereby there was a significant increase in hydrolysis rate at or above pH 9. 16,20,22 We posit that our experimental pH values of 5.0 and 7.0 were too low for us to observe the effects of base-catalyzed hydrolysis. Our measured  $t_{1/2}$  (12 d) for cephalexin at pH 7.0 (25 °C) was over sixfold faster than the previously reported value ( $t_{1/2}$  75–86 d; pH 8, 35 °C) by Yamana and Tsuji, 82 despite the fact that a relatively higher temperature was expected to increase the degradation rate of  $\beta$ -lactams. <sup>22,83</sup> Interestingly, we did not observe significant hydrolysis of amoxicillin, despite a number of studies reporting hydrolysis rates observable on our timescale at pH 5.0  $(t_{1/2} = 14.5 \text{ d})^{19}$  and pH 7.0  $(t_{1/2} = 6.0 \text{ d}, ^{25} 12.5 \text{ d}, ^{19} 18 \text{ d}, ^{84}$  and 20 d<sup>4</sup>). Hydrolysis rate constants for other  $\beta$ lactam antibiotics in the cephem and penam families have been reported with  $t_{1/2}$  values ranging from 1.4 to 9.7 d for the cephems<sup>20–22</sup> and 1.0–36 d for the penams<sup>22,23</sup> under similar experimental conditions (circumneutral pH, shielded from light). We used HPLC-DAD and MS to characterize the observed hydrolysis products. For cephalexin hydrolysis, our data implied the removal of the conjugated benzene and cephem groups. For ceftriaxone hydrolysis, we obtained two previously reported products, thiotriazinone and 3-desacetyl cefotaxime,  $^{24,76}$  and a previously unreported ion (m/z =261.0652, z = +1) with a suggested composition of C<sub>8</sub>H<sub>13</sub>O<sub>4</sub>N<sub>4</sub>S<sup>+</sup>. Further investigation is needed to confirm the identity of this ion because we were not able to resolve the specific chemical structure based on our data.

With respect to the interaction of different antibiotics with clay particles suspended in solution, cephalexin displayed a slightly higher affinity for montmorillonite than amoxicillin at pH 5.0. Amoxicillin and cephalexin had similar affinities for montmorillonite at pH 7.0, which were significantly higher than the affinity of ceftriaxone for montmorillonite at the same pH. Overall, we obtained greater amounts (up to 9-fold) of adsorbed compounds at pH 7.0 than at pH 5.0. The increased affinity for  $\beta$ -lactams to montmorillonite at higher pH contrasted previous reports of pH-dependent adsorption on montmorillonite for other classes of antibiotics, such as tetracyclines, 42-45 fluoroquinolones, 50 and sulfonamides. 39 However, despite the relatively lower extent of adsorption at pH 7.0 compared to acidic pH in these previous studies with other antibiotics, the amount adsorbed per gram of clay was still up to 300-fold higher than what we obtained here with  $\beta$ lactam antibiotics. The low affinity of smectite clays for  $\beta$ lactam antibiotics at circumneutral pH was previously reported (removal efficiency <10%). <sup>33,85</sup> Our XRD data implied that the relatively low amounts of adsorbed  $\beta$ -lactam compounds are localized primarily on the external basal surfaces and clay edges, instead of being trapped within the interlayer spacings of the smectite clay.

Poor adsorption of  $\beta$ -lactams to adsorbents such as clays and activated carbon at circumneutral pH has been attributed to the low hydrophobicity and negatively charged species of these antibiotics. Furthermore, cation bridging through the presence of multivalent metal cations in solution can be important to promote adsorption of negatively charged antibiotics on negatively charged clay surfaces. Accordingly, it was shown that augmentation of bentonite clay with Fe and Ni was required for a 70% increase in retention of

ampicillin, amoxicillin, and penicillin.<sup>34</sup> Also, montmorillonite modified by a bound cationic surfactant (didodecyldimethylammonium) exhibited increased removal efficiency (from less than 10% to over 90%) of penams (penicillin G and nafcillin) and cephems (cefazolin and cefotaxime) from wastewater,<sup>33</sup> further highlighting the importance of organic or inorganic cations in facilitating the adsorption of  $\beta$ -lactams on clays.

We used molecular modeling simulations to predict thermodynamically favorable conformations at pH 7.0 for the adsorption of the different antibiotics on the basal clay surfaces, which involved a network of electrostatic interactions (through the protonated amino group) and both direct and water-bridged hydrogen bonds. Based on their chemical structures (Figure 1), the  $\beta$ -lactam antibiotics investigated here are either negatively charged and/or zwitterionic species in solution at pH 7.0. Based on the intermolecular interactions with the clay surface, our simulations revealed that the negatively charged cephalexin exhibited the weakest affinity for the montmorillonite clay, followed by the zwitterionic amoxicillin and zwitterionic cephalexin with the highest affinity. In addition to the basal surfaces modeled in our simulations, we acknowledge that the clay edge sites may be involved in clay-antibiotic interactions. 88,89 However, we have focused on simulating adsorption interactions on the basal clay surfaces because the basal surfaces are expected to be preferred adsorption sites over the clay edges, as demonstrated by metadynamics of simulated interactions of phthalate esters with montmorillonite.90

At pH 7.0, we investigated the effects of DOM on the claymediated removal of amoxicillin (a penam) or ceftriaxone (a cephem) from solution, given that DOM is known to adsorb to clays.  $^{91-93}$  In the presence of DOM (from 10 to 100 mg L<sup>-1</sup>), there was either no change or only a 10% decrease in the removal of amoxicillin by the clay, but, by contrast, the DOM completely impeded the adsorption of ceftriaxone. Based on the acid-base chemistry at pH 7.0 (Figure 1), ceftriaxone in solution exists primarily as divalent anions and amoxicillin primarily as zwitterionic, which may explain the relatively higher interfering effects of DOM on the adsorption of ceftriaxone than the adsorption of amoxicillin. A previous study on DOM interactions with fluoroquinolone antibiotics revealed that van der Waals interactions including hydrogen bonding were favorable for complexes of these antibiotics by DOM. 48-50 In a similar fashion, hydrogen bonding of DOM with both the montmorillonite surface and with the antibiotics in solution may interfere with the binding of the antibiotics on the montmorillonite surface. The mechanistic role of multivalent cations in bridging interactions between clay, NOM, and  $\beta$ -lactams remains to be resolved. Moreover, while we did not investigate the role of light-mediated degradation in the presence of DOM, previous studies have already demonstrated DOM-enhanced photolysis of  $\beta$ -lactam antibiotics. <sup>21,81,84</sup> Taken together our findings and previously published findings, we concluded that the presence of DOM in solution may both interfere with mineral capture of  $\beta$ -lactams out of solution and promote photolysis in solution, depending on the structure of the  $\beta$ -lactams in solution.

## 5. CONCLUSIONS

In summary, we observed that degradation only occurred for the cephem antibiotics (ceftriaxone at pH 5.0 and cephalexin at pH 7.0), indicating that the cephem subgroup of  $\beta$ -lactams is more easily degraded than penam subgroup. Using HPLC–UV

and HPLC-DAD analysis, we identified two hydrolysis products for ceftriaxone, which we confirmed to be thiotriazinone and 3-desacetyl cefotaxime using high-resolution MS. From our chromatographic analysis, we were able to ascertain that the conjugated benzene and cephem moieties were removed from cephalexin during hydrolysis reactions. However, we were not able to resolve the final structure of the hydrolysis products using MS analysis. Adsorption experiments with smectite clay particles revealed that there was a 4- to 9fold higher adsorption at circumneutral pH than at acidic pH for the antibiotics investigated, but the extent of adsorption was dependent on the antibiotic structures. For instance, at the acidic pH, there was greater adsorption of cephalexin (a cephem) than amoxicillin (a penam), but at circumneutral pH 7.0, there was greater adsorption of both cephalexin and amoxicillin than ceftriaxone (a cephem). The XRD data indicated that the antibiotics were not trapped within the interlayer nanopores but adsorbed primarily on the external surfaces of the clay particles. Molecular modeling simulations revealed different adsorption mechanisms for the different types of antibiotics, whereby the participation of positively charged amino group and a network of hydrogen bonds led to favorable adsorbate conformations. Interestingly, when the solution contained DOM, there was minimal effect on the adsorption of amoxicillin (a penam) onto the clay surface, but there was up to 100% inhibition in the adsorption of ceftriaxone (a cephem), implying that different intermolecular interactions with different structures of  $\beta$ -lactams antibiotics may dictate the extent of DOM effects on the antibiotic interactions with mineral particles suspended in solution.

#### ASSOCIATED CONTENT

### Supporting Information

The Supporting Information is available free of charge at https://pubs.acs.org/doi/10.1021/acsearthspace-chem.1c00064.

Detailed experimental methodology, force-field validation simulations with amoxicillin, force-field validation simulations with cephalexin, kinetics of solution concentration in the absence (control) and presence of montmorillonite, chromatograms from HPLC–UV analysis, two time-point hydrolysis experiment results: comparison between buffer and water matrices, m/z spectra from the direct infusion of  $\beta$ -lactam antibiotics at pH 5 and pH 7 in a water solution, top 20 exported ions in water matrix controls and experimental samples, theoretical parent compounds with common adducts, Freundlich fitting model parameters, and FTIR spectra of  $\beta$ -lactam antibiotics equilibrated with montmorillonite (PDF)

## AUTHOR INFORMATION

## **Corresponding Author**

Ludmilla Aristilde — Department of Civil and Environmental Engineering, McCormick School of Engineering and Applied Science, Northwestern University, Evanston, Illinois 60208, United States; Department of Biological and Environmental Engineering, College of Agriculture and Life Sciences, Department of Civil and Environmental Engineering, College of Engineering, and Soil and Crop Sciences Section, School of Integrative Plant Science, College of Agriculture and Life Sciences, Cornell University, Ithaca, New York 14853, United

States; o orcid.org/0000-0002-8566-1486; Phone: 847-491-2999; Email: ludmilla.aristilde@northwestern.edu

#### **Authors**

- Annaleise R. Klein Department of Civil and Environmental Engineering, McCormick School of Engineering and Applied Science, Northwestern University, Evanston, Illinois 60208, United States; Department of Biological and Environmental Engineering, College of Agriculture and Life Sciences, Cornell University, Ithaca, New York 14853, United States; Present Address: Australian Synchrotron, Australian Nuclear Science and Technology Organisation, Clayton, VIC 3168 Australia.
- Eirini Sarri Department of Civil and Environmental Engineering, College of Engineering, Cornell University, Ithaca, New York 14853, United States
- Sabrina E. Kelch Soil and Crop Sciences Section, School of Integrative Plant Science, College of Agriculture and Life Sciences, Cornell University, Ithaca, New York 14853, United States
- Jade J. Basinski Department of Civil and Environmental Engineering, McCormick School of Engineering and Applied Science, Northwestern University, Evanston, Illinois 60208, United States
- Shreya Vaidya Department of Chemical and Biomolecular Engineering, College of Engineering, Cornell University, Ithaca, New York 14853, United States

Complete contact information is available at: https://pubs.acs.org/10.1021/acsearthspacechem.1c00064

#### **Author Contributions**

 $\P$ A.R.K. and E.S.Co-first authors.

#### Notes

The authors declare no competing financial interest.

## ACKNOWLEDGMENTS

Research funding was provided by a CAREER grant (CBET-1653092) from the U.S. National Science Foundation and Northwestern University. We acknowledge the Northwestern Integrated Molecular Structure Education and Research Center (IMSERC), which is supported by the Soft and Hybrid Nanotechnology Experimental (SHyNE) Resource (NSF ECCS-1542205), the State of Illinois, and the International Institute for Nanotechnology (IIN). We are grateful for the assistance of Ananya Gangadhar and Fanny Okaikue-Woodi in obtaining preliminary data during the early stages of this work and Krista Barzen-Hanson for HPLC method development.

## REFERENCES

- (1) Mitić, N.; Miraula, M.; Selleck, C.; Hadler, K. S.; Uribe, E.; Pedroso, M. M.; Schenk, G. Chapter Three Catalytic Mechanisms of Metallohydrolases Containing Two Metal Ions. In *Advances in Protein Chemistry and Structural Biology*; Christov, C. Z., Ed.; Academic Press, 2014; Vol. 97, pp 49–81.
- (2) Bailón-Pérez, M. I.; García-Campaña, A. M.; del Olmo-Iruela, M.; Gámiz-Gracia, L.; Cruces-Blanco, C. Trace determination of  $10~\beta$ -lactam antibiotics in environmental and food samples by capillary liquid chromatography. *J. Chromatogr. A* **2009**, *1216*, 8355–8361.
- (3) Rodriguez-Herrera, R.; Puc, L. E. C.; Sobrevilla, J. M. V.; Luque, D.; Cardona-Felix, C. S.; Aguilar-González, C. N.; Flores-Gallegos, A. C. Enzymes in the Pharmaceutical Industry for  $\beta$ -Lactam Antibiotic Production. In *Enzymes in Food Biotechnology*; Kuddus, M., Ed.; Academic Press, 2019; pp 627–643.

- (4) Braschi, I.; Blasioli, S.; Fellet, C.; Lorenzini, R.; Garelli, A.; Pori, M.; Giacomini, D. Persistence and degradation of new  $\beta$ -lactam antibiotics in the soil and water environment. *Chemosphere* **2013**, 93, 152–159
- (5) Cha, J. M.; Yang, S.; Carlson, K. H. Trace determination of  $\beta$ -lactam antibiotics in surface water and urban wastewater using liquid chromatography combined with electrospray tandem mass spectrometry. *J. Chromatogr. A* **2006**, *1115*, 46–57.
- (6) Christian, T.; Schneider, R. J.; Färber, H. A.; Skutlarek, D.; Meyer, M. T.; Goldbach, H. E. Determination of Antibiotic Residues in Manure, Soil, and Surface Waters. *Acta Hydrochim. Hydrobiol.* **2003**, *31*, 36–44.
- (7) Li, D.; Yang, M.; Hu, J.; Zhang, Y.; Chang, H.; Jin, F. Determination of penicillin G and its degradation products in a penicillin production wastewater treatment plant and the receiving river. *Water Res.* **2008**, 42, 307–317.
- (8) Kümmerer, K.; Henninger, A. Promoting resistance by the emission of antibiotics from hospitals and households into effluent. *Clin. Microbiol. Infect.* **2003**, *9*, 1203–1214.
- (9) Kümmerer, K. Antibiotics in the aquatic environment A review Part I. *Chemosphere* **2009**, *75*, 417–434.
- (10) Bush, K.; Bradford, P. A.  $\beta$ -Lactams and  $\beta$ -Lactamase Inhibitors: An Overview. *Cold Spring Harbor Perspect. Med.* **2016**, 6, a025247.
- (11) Kong, K.-F.; Schneper, L.; Mathee, K. Beta-lactam antibiotics: from antibiosis to resistance and bacteriology. *APMIS* **2010**, *118*, 1–36.
- (12) Gallagher, J. C.; MacDougall, C., Beta-Lactams. In *Antibiotics Simplified*, 4th ed.; Jones & Bartlett Learning: Burlington, MA, 2017.
- (13) Bennett, J. E.; Dolin, R.; Blaser, M. J., Mandell, Douglas, and Bennett's Principles and Practice of Infectious Diseases, 8th ed.; Elsevier Inc.: Philadelphia, PA, 2015.
- (14) Bush, K. Past and Present Perspectives on  $\beta$ -Lactamases. Antimicrob. Agents Chemother. 2018, 62, No. e01076.
- (15) Cycoń, M.; Mrozik, A.; Piotrowska-Seget, Z. Antibiotics in the Soil Environment-Degradation and Their Impact on Microbial Activity and Diversity. *Front. Microbiol.* **2019**, *10*, 338.
- (16) Chen, J.; Sun, P.; Zhou, X.; Zhang, Y.; Huang, C.-H. Cu(II)-Catalyzed Transformation of Benzylpenicillin Revisited: The Overlooked Oxidation. *Environ. Sci. Technol.* **2015**, 49, 4218–4225.
- (17) Zhang, X.; Guo, Y.; Pan, Y.; Yang, X. Distinct effects of copper on the degradation of  $\beta$ -lactam antibiotics in fulvic acid solutions during light and dark cycle. *Environ. Sci. Ecotechnol.* **2020**, 3, 100051.
- (18) Hsu, M.-H.; Kuo, T.-H.; Wei-Po Lai, W.; Huang, C.-H.; Hsu, C.-C.; Chen, Y.-E.; Lin, A. Y.-C. Effect of environmental factors on the oxidative transformation of cephalosporin antibiotics by manganese dioxides. *Environ. Sci.: Processes Impacts* **2019**, *21*, 692–700
- (19) Chadha, R.; Kashid, N.; Jain, D. V. S. Kinetic studies of the degradation of an aminopenicillin antibiotic (amoxicillin trihydrate) in aqueous solution using heat conduction microcalorimetry. *J. Pharm. Pharmacol.* **2010**, *55*, 1495–1503.
- (20) Ribeiro, A. R.; Lutze, H. V.; Schmidt, T. C. Base-catalyzed hydrolysis and speciation-dependent photolysis of two cephalosporin antibiotics, ceftiofur and cefapirin. *Water Res.* **2018**, *134*, 253–260.
- (21) Jiang, M.; Wang, L.; Ji, R. Biotic and abiotic degradation of four cephalosporin antibiotics in a lake surface water and sediment. *Chemosphere* **2010**, *80*, 1399–1405.
- (22) Mitchell, S. M.; Ullman, J. L.; Teel, A. L.; Watts, R. J. pH and temperature effects on the hydrolysis of three  $\beta$ -lactam antibiotics: Ampicillin, cefalotin and cefoxitin. *Sci. Total Environ.* **2014**, 466–467, 547–555.
- (23) Timm, A.; Borowska, E.; Majewsky, M.; Merel, S.; Zwiener, C.; Bräse, S.; Horn, H. Photolysis of four  $\beta$ lactam antibiotics under simulated environmental conditions: Degradation, transformation products and antibacterial activity. *Sci. Total Environ.* **2019**, *651*, 1605–1612.
- (24) Abramović, B. F.; Uzelac, M. M.; Armaković, S. J.; Gašić, U.; Četojević-Simin, D. D.; Armaković, S. Experimental and computa-

- tional study of hydrolysis and photolysis of antibiotic ceftriaxone: Degradation kinetics, pathways, and toxicity. *Sci. Total Environ.* **2021**, 768, 144991.
- (25) Hirte, K.; Seiwert, B.; Schüürmann, G.; Reemtsma, T. New hydrolysis products of the beta-lactam antibiotic amoxicillin, their pH-dependent formation and search in municipal wastewater. *Water Res.* **2016**, *88*, 880–888.
- (26) Dudkowska, J.; Frańska, M.; Frański, R. Detection of the iron complexes with hydrolysis products of cephalexin and cefradine upon high-performance liquid chromatography/electrospray ionization mass spectrometry analysis. *Rapid Commun. Mass Spectrom.* **2018**, 32, 576–582.
- (27) Coşkun, E.; Duman, E.; Acar, N.; Biçer, E. Electrochemical, Spectroscopic and Computational Studies on Complexation of Oxacillin with Cu (II) and Co (II) ions. Synthesis and Ligand Hydrolysis. *Int. J. Electrochem. Sci.* **2017**, *12*, 9364–9377.
- (28) Sheng, F.; Ling, J.; Wang, C.; Jin, X.; Gu, X.; Li, H.; Zhao, J.; Wang, Y.; Gu, C. Rapid Hydrolysis of Penicillin Antibiotics Mediated by Adsorbed Zinc on Goethite Surfaces. *Environ. Sci. Technol.* **2019**, 53, 10705–10713.
- (29) Guo, Y.; Tsang, D. C. W.; Zhang, X.; Yang, X. Cu(II)-catalyzed degradation of ampicillin: effect of pH and dissolved oxygen. *Environ. Sci. Pollut. Res.* **2018**, 25, 4279–4288.
- (30) Huang, T.; Fang, C.; Qian, Y.; Gu, H.; Chen, J. Insight into Mn(II)-mediated transformation of  $\beta$ -lactam antibiotics: The overlooked hydrolysis. *Chem. Eng. J.* **2017**, 321, 662–668.
- (31) Chen, J.; Wang, Y.; Qian, Y.; Huang, T. Fe(III)-promoted transformation of  $\beta$ -lactam antibiotics: Hydrolysis vs oxidation. *J. Hazard. Mater.* **2017**, 335, 117–124.
- (32) Chen, J.; Sun, P.; Zhang, Y.; Huang, C.-H. Multiple Roles of Cu(II) in Catalyzing Hydrolysis and Oxidation of  $\beta$ -Lactam Antibiotics. *Environ. Sci. Technol.* **2016**, 50, 12156–12165.
- (33) Saitoh, T.; Shibayama, T. Removal and degradation of  $\beta$ -lactam antibiotics in water using didodecyldimethylammonium bromide-modified montmorillonite organoclay. *J. Hazard. Mater.* **2016**, 317, 677–685
- (34) Weng, X.; Cai, W.; Lan, R.; Sun, Q.; Chen, Z. Simultaneous removal of amoxicillin, ampicillin and penicillin by clay supported Fe/Ni bimetallic nanoparticles. *Environ. Pollut.* **2018**, 236, 562–569.
- (35) Tri, N. N.; Nguyen, M. T.; Trung, N. T. A molecular level insight into adsorption of  $\beta$ -lactam antibiotics on vermiculite surface. *Surf. Sci.* **2020**, 695, 121588.
- (36) Ahmed, A. A.; Thiele-Bruhn, S.; Leinweber, P.; Kühn, O. Towards a molecular level understanding of the sulfanilamide-soil organic matter-interaction. *Sci. Total Environ.* **2016**, *559*, 347–355.
- (37) Chen, K.-L.; Liu, L.-C.; Chen, W.-R. Adsorption of sulfamethoxazole and sulfapyridine antibiotics in high organic content soils. *Environ. Pollut.* **2017**, 231, 1163–1171.
- (38) Schwarz, J.; Thiele-Bruhn, S.; Eckhardt, K.-U.; Schulten, H.-R. Sorption of sulfonamide antibiotics to soil organic sorbents: batch experiments with model compounds and computational chemistry. *ISRN Soil Sci.* **2012**, 2012, 159189.
- (39) Gao, J.; Pedersen, J. A. Adsorption of sulfonamide antimicrobial agents to clay minerals. *Environ. Sci. Technol.* **2005**, 39, 9509–9516.
- (40) Gao, J.; Pedersen, J. A. Sorption of Sulfonamide Antimicrobial Agents to Humic Acid-Clay Complexes. *J. Environ. Qual.* **2010**, *39*, 228–235.
- (41) Thiele-Bruhn, S.; Seibicke, T.; Schulten, H.-R.; Leinweber, P. Sorption of Sulfonamide Pharmaceutical Antibiotics on Whole Soils and Particle-Size Fractions. *J. Environ. Qual.* **2004**, *33*, 1331–1342.
- (42) Li, Z.; Chang, P.-H.; Jean, J.-S.; Jiang, W.-T.; Wang, C.-J. Interaction between tetracycline and smectite in aqueous solution. *J. Colloid Interface Sci.* **2010**, 341, 311–319.
- (43) Aristilde, L.; Lanson, B.; Charlet, L. Interstratification Patterns from the pH-Dependent Intercalation of a Tetracycline Antibiotic within Montmorillonite Layers. *Langmuir* **2013**, *29*, 4492–4501.
- (44) Aristilde, L.; Lanson, B.; Miéhé-Brendlé, J.; Marichal, C.; Charlet, L. Enhanced interlayer trapping of a tetracycline antibiotic

- within montmorillonite layers in the presence of Ca and Mg. J. Colloid Interface Sci. 2016, 464, 153–159.
- (45) Aristilde, L.; Marichal, C.; Miéhé-Brendlé, J.; Lanson, B.; Charlet, L. Interactions of Oxytetracycline with a Smectite Clay: A Spectroscopic Study with Molecular Simulations. *Environ. Sci. Technol.* **2010**, *44*, 7839–7845.
- (46) Conde-Cid, M.; Ferreira-Coelho, G.; Núñez-Delgado, A.; Fernández-Calviño, D.; Arias-Estévez, M.; Álvarez-Rodríguez, E.; Fernández-Sanjurjo, M. J. Competitive adsorption of tetracycline, oxytetracycline and chlortetracycline on soils with different pH value and organic matter content. *Environ. Res.* **2019**, *178*, 108669.
- (47) Zhang, D.; Yang, S.; Wang, Y.; Yang, C.; Chen, Y.; Wang, R.; Wang, Z.; Yuan, X.; Wang, W. Adsorption characteristics of oxytetracycline by different fractions of organic matter in sedimentary soil. *Environ. Sci. Pollut. Res.* **2019**, *26*, 5668–5679.
- (48) Aristilde, L.; Sposito, G. Complexes of the antimicrobial ciprofloxacin with soil, peat, and aquatic humic substances. *Environ. Toxicol. Chem.* **2013**, 32, 1467–1478.
- (49) Aristilde, L.; Sposito, G. Binding of ciprofloxacin by humic substances: A molecular dynamics study. *Environ. Toxicol. Chem.* **2010**, 29, 90–98.
- (50) Okaikue-Woodi, F. E. K.; Kelch, S. E.; Schmidt, M. P.; Enid Martinez, C.; Youngman, R. E.; Aristilde, L. Structures and mechanisms in clay nanopore trapping of structurally-different fluoroquinolone antimicrobials. *J. Colloid Interface Sci.* **2018**, *513*, 367–378.
- (51) Zhang, H.; Lu, T.; Zhang, R.; Wang, M.; Krishnan, S.; Liu, S.; Zhou, Y.; Li, D.; Qi, Z. Effects of clay colloids on ciprofloxacin transport in saturated quartz sand porous media under different solution chemistry conditions. *Ecotoxicol. Environ. Saf.* **2020**, 199, 110754.
- (52) Duan, W.; Wang, N.; Xiao, W.; Zhao, Y.; Zheng, Y. Ciprofloxacin adsorption onto different micro-structured tourmaline, halloysite and biotite. *J. Mol. Liq.* **2018**, *269*, 874–881.
- (53) Demiralay, E. Ç.; Koç, D.; Daldal, Y. D.; Çakır, C. Determination of chromatographic and spectrophotometric dissociation constants of some beta lactam antibiotics. *J. Pharm. Biomed. Anal.* **2012**, *71*, 139–143.
- (54) Demiralay, E. Ç.; Üstün, Z.; Daldal, Y. D. Estimation of thermodynamic acidity constants of some penicillinase-resistant penicillins. *J. Pharm. Biomed. Anal.* **2014**, *91*, 7–11.
- (55) Mrestani, Y.; Neubert, R.; Munk, A.; Wiese, M. Determination of dissociation constants of cephalosporins by capillary zone electrophoresis. *J. Chromatogr. A* **1998**, 803, 273–278.
- (56) Aleksić, M.; Savić, V.; Popović, G.; Burić, N.; Kapetanović, V. Acidity constants of cefetamet, cefotaxime and ceftriaxone; the effect of the substituent at C3 position. *J. Pharm. Biomed. Anal.* **2005**, 39, 752–756.
- (57) Längin, A.; Alexy, R.; König, A.; Kümmerer, K. Deactivation and transformation products in biodegradability testing of β-lactams amoxicillin and piperacillin. *Chemosphere* **2009**, *75*, 347–354.
- (58) Subbiah, M.; Mitchell, S. M.; Ullman, J. L.; Call, D. R.  $\beta$ -Lactams and Florfenicol Antibiotics Remain Bioactive in Soils while Ciprofloxacin, Neomycin, and Tetracycline Are Neutralized. *Appl. Environ. Microbiol.* **2011**, *77*, 7255–7260.
- (59) Szekeres, E.; Chiriac, C. M.; Baricz, A.; Szőke-Nagy, T.; Lung, I.; Soran, M.-L.; Rudi, K.; Dragos, N.; Coman, C. Investigating antibiotics, antibiotic resistance genes, and microbial contaminants in groundwater in relation to the proximity of urban areas. *Environ. Pollut.* **2018**, 236, 734–744.
- (60) Bergheim, M.; Helland, T.; Kallenborn, R.; Kümmerer, K. Benzyl-penicillin (Penicillin G) transformation in aqueous solution at low temperature under controlled laboratory conditions. *Chemosphere* **2010**, *81*, 1477–1485.
- (61) King, R.; Bonfiglio, R.; Fernandez-Metzler, C.; Miller-Stein, C.; Olah, T. Mechanistic investigation of ionization suppression in electrospray ionization. *J. Am. Soc. Mass Spectrom.* **2000**, *11*, 942–950.
- (62) Naegele, E. Making Your LC Method Compatible with Mass Spectrometry; Agilent Technologies: Waldbronn, Germany, 2011.

- (63) BIOVIA. Materials Studio; Dassault Systèmes: San Diego, 2020.
- (64) BIOVIA. Discovery Studio; Dassault Systèmes: San Diego, 2020.
- (65) Pochodylo, A. L.; Aoki, T. G.; Aristilde, L. Adsorption mechanisms of microcystin variant conformations at water-mineral interfaces: A molecular modeling investigation. *J. Colloid Interface Sci.* **2016**, 480, 166–174.
- (66) Boles, M. O.; Girven, R. J.; Gane, P. A. C. The structure of amoxycillin trihydrate and a comparison with the structures of ampicillin. *Acta Crystallogr., Sect. B: Struct. Sci.* 1978, 34, 461–466.
- (67) Kennedy, A. R.; Okoth, M. O.; Sheen, D. B.; Sherwood, J. N.; Teat, S. J.; Vrcelj, R. M. Cephalexin: a channel hydrate. *Acta Crystallogr., Sect. C: Cryst. Struct. Commun.* **2003**, *59*, o650–o652.
- (68) Aristilde, L.; Galdi, S. M.; Kelch, S. E.; Aoki, T. G. Sugar-influenced water diffusion, interaction, and retention in clay interlayer nanopores probed by theoretical simulations and experimental spectroscopies. *Adv. Water Resour.* **2017**, *106*, 24–38.
- (69) Klein, A. R.; Bone, S. E.; Bakker, E.; Chang, Z.; Aristilde, L. Abiotic phosphorus recycling from adsorbed ribonucleotides on a ferrihydrite-type mineral: Probing solution and surface species. *J. Colloid Interface Sci.* **2019**, 547, 171–182.
- (70) Mähler, J.; Persson, I. A study of the hydration of the alkali metal ions in aqueous solution. *Inorg. Chem.* **2012**, *51*, 425–438.
- (71) Panda, S. S.; Ravi Kumar, B. V.; Dash, R.; Mohanta, G. Determination of cephalexin monohydrate in pharmaceutical dosage form by stability-indicating RP-UFLC and UV spectroscopic methods. *Sci. Pharm.* **2013**, *81*, 1029–1041.
- (72) Vilanova, B.; Muñoz, F.; Donoso, J.; Blanco, F. G. Analysis of the UV Absorption Band of Cephalosporins. *Appl. Spectrosc.* **1992**, *46*, 44–48.
- (73) Thomas, P. W.; Cammarata, M.; Brodbelt, J. S.; Fast, W. Covalent Inhibition of New Delhi Metallo- $\beta$ -Lactamase-1 (NDM-1) by Cefaclor. *ChemBioChem* **2014**, *15*, 2541–2548.
- (74) Grant, A.; Bhattacharyya, P. K. Application of derivative spectroscopy to the determination of chromatographic peak purity. *J. Chromatogr. A* **1985**, 347, 219–235.
- (75) Abramovic, B.; Uzelac, M.; Fincur, N. Photocatalytic degradation of thiotriazinone, stable hydrolysis product of antibiotic ceftriaxone. *Acta Period. Technol.* **2019**, 50, 1–11.
- (76) Tian, Y.; Lu, L.; Chang, Y.; Zhang, D.-s.; Li, J.; Feng, Y.-C.; Hu, C.-Q. Identification of a new isomer from a reversible isomerization of ceftriaxone in aqueous solution. *J. Pharm. Biomed. Anal.* **2015**, *102*, 326–330.
- (77) Barone, R.; Chanon, M.; Gallo, R. Aminothiazoles and Their Derivatives; *Chemistry of Heterocyclic Compounds*; John Wiley & Sons, Ltd, 1979; Vol. 34, p 9-368.
- (78) Kloprogge, J. T.; Mahmutagic, E.; Frost, R. L. Mid-infrared and infrared emission spectroscopy of Cu-exchanged montmorillonite. *J. Colloid Interface Sci.* **2006**, 296, 640–646.
- (79) Tyagi, B.; Chudasama, C. D.; Jasra, R. V. Determination of structural modification in acid activated montmorillonite clay by FT-IR spectroscopy. *Spectrochim. Acta, Part A* **2006**, *64*, 273–278.
- (80) de Diego Glaría, M.; Moscciati, G. G.; Ramos, R. G.; Riquelme, M. M. Stability of ceftriaxone in water and cerebrospinal fluid determined by high-performance liquid chromatography. *J. Sep. Sci.* **2003**, *26*, 939–942.
- (81) Kedzierewicz, F.; Finance, C.; Nicolas, A.; Dixneuf, P.; Hoffman, M. Stability of parenteral ceftriaxone disodium solutions in frozen and liquid states: Effect of freezing and microwave thawing. *J. Pharm. Sci.* **1989**, *78*, 73–77.
- (82) Yamana, T.; Tsuji, A. Comparative stability of cephalosporins in aqueous solution: kinetics and mechanisms of degradation. *J. Pharm. Sci.* **1976**, *65*, 1563–1574.
- (83) do Nascimento, T. G.; de Jesus Oliveira, E.; Basílio Júnior, I. D.; de Araújo-Júnior, J. X.; Macêdo, R. O. Short-term stability studies of ampicillin and cephalexin in aqueous solution and human plasma: Application of least squares method in Arrhenius equation. *J. Pharm. Biomed. Anal.* **2013**, *73*, 59–64.

- (84) Xu, H.; Cooper, W. J.; Jung, J.; Song, W. Photosensitized degradation of amoxicillin in natural organic matter isolate solutions. *Water Res.* **2011**, *45*, 632–638.
- (85) Weng, X.; Sun, Q.; Lin, S.; Chen, Z.; Megharaj, M.; Naidu, R. Enhancement of catalytic degradation of amoxicillin in aqueous solution using clay supported bimetallic Fe/Ni nanoparticles. *Chemosphere* **2014**, *103*, 80–85.
- (86) Gu, C.; Karthikeyan, K. G.; Sibley, S. D.; Pedersen, J. A. Complexation of the antibiotic tetracycline with humic acid. *Chemosphere* **2007**, *66*, 1494–1501.
- (87) Avisar, D.; Primor, O.; Gozlan, I.; Mamane, H. Sorption of sulfonamides and tetracyclines to montmorillonite clay. *Water, Air, Soil Pollut.* **2010**, 209, 439–450.
- (88) Liu, X.; Lu, X.; Sprik, M.; Cheng, J.; Meijer, E. J.; Wang, R. Acidity of edge surface sites of montmorillonite and kaolinite. *Geochim. Cosmochim. Acta* 2013, 117, 180–190.
- (89) Tombácz, E.; Nyilas, T.; Libor, Z.; Csanaki, C. Surface charge heterogeneity and aggregation of clay lamellae in aqueous suspensions. *From Colloids to Nanotechnology*; Springer, 2004; pp 206–215.
- (90) Willemsen, J. A. R.; Myneni, S. C. B.; Bourg, I. C. Molecular dynamics simulations of the adsorption of phthalate esters on smectite clay surfaces. *J. Phys. Chem. C* **2019**, *123*, 13624–13636.
- (91) Derakhshani, E.; Naghizadeh, A. Optimization of humic acid removal by adsorption onto bentonite and montmorillonite nanoparticles. *J. Mol. Liq.* **2018**, 259, 76–81.
- (92) Chen, H.; Koopal, L. K.; Xiong, J.; Avena, M.; Tan, W. Mechanisms of soil humic acid adsorption onto montmorillonite and kaolinite. *J. Colloid Interface Sci.* **2017**, *504*, 457–467.
- (93) Feng, X.; Simpson, A. J.; Simpson, M. J. Chemical and mineralogical controls on humic acid sorption to clay mineral surfaces. *Org. Geochem.* **2005**, *36*, 1553–1566.